ISSN: 0067-2904

A Comparative Study on the Photocatalytic Degradation of Doxycycline Antibiotic in the Presence of ZnO/g-C_3N_4 and TiO_2/g-C_3N_4 Composites

Nguyen Thanh Tuoi[1], Bui Thi Minh Nguyet[2],Dinh Quang Khieu[1], Nguyen Van Hung[2]*
[1] *University of Sciences, Hue University, Hue, 49000, Vietnam*
[2] *Faculty of Natural Sciences, Dong Thap University, Dong Thap, 81000, Vietnam*

Received: 10/3/2024 Accepted: 13/11/2024 Published: 30/11/2025

Abstract

This study employed a simple hydrolysis method to synthesize two novel nanocomposites: ZnO/g-C_3N_4 (ZCN) and TiO_2/g-C_3N_4 (TCN). Characterization results confirmed the successful integration of ZnO and TiO_2 nanoparticles onto g-C_3N_4 nanosheets, resulting in enhanced optical absorption in the visible light region. Both synthesized ZCN and TCN composites exhibited higher photocatalytic degradation efficiency of the antibiotic doxycycline under visible light irradiation compared to their individual component materials. This enhancement is attributed to the formation of heterojunction between TiO_2 or ZnO and porous g-C_3N_4, which improves electron-hole pair separation and reduces recombination. The photocatalytic degradation kinetics of doxycycline using ZCN and TCN followed a pseudo-first-order model, with both catalysts demonstrating operational stability and effectiveness in antibiotic photodegradation.

Keywords: Zinc oxide, Graphitic carbon nitride, Biochar, Photodegradation, Doxycycline.

1. Introduction

Doxycycline hydrochloride (DC) is a semi-synthetic tetracycline antibiotic. The direct discharge of various antibiotics, such as doxycycline (DC), into the environment poses significant risks to ecosystems and human health. Therefore, proposing effective solutions for treating wastewater containing antibiotics is essential [1, 2]. Among various wastewater treatment techniques, Advanced Oxidation Processes (AOPs) assisted by photocatalysts have garnered significant attention from researchers worldwide due to their high efficiency [1, 2]. When the photocatalyst is activated by a light source of appropriate energy, it generates free radicals that can effectively photodegrade organic pollutants [3]. However, this process is often hindered by low solar energy utilization, rapid recombination of photogenerated electron-hole pairs, and photodegradation of photocatalytic semiconductor materials. Many photocatalysts such as TiO_2, ZnO, WO_3, CdS, CuO and BiOCl have been effectively used to treat various organic pollutants [4-9].

Among various photocatalysts, TiO_2 and ZnO have been recognized for their effectiveness in treating wastewater containing pharmaceuticals due to their excellent properties, including non-toxicity, durability, low cost, and strong UV absorption capability [5]. However, both TiO_2 and ZnO have large band gaps (about 3.2 eV for TiO_2 and 3.37 eV for ZnO), which

*Email: nguyen.vt.gt@gmail.com

restrict their photocatalytic activity to the near-ultraviolet light region. Furthermore, they have low photocatalytic degradation efficiency due to the rapid recombination of photogenerated electron/hole pairs [10-12]. Consequently, numerous studies have aimed to enhance the visible light absorption and effectively separate electron-hole pairs of TiO_2 and ZnO. This can be achieved through metal ion doping [13, 14], surface modification [15, 16], and heterogeneous structural design [17, 18]. Among these approaches, coupling graphitic carbon nitride (g-C_3N_4) with other semiconductors possessing suitable band gap energies can enhance light absorption, improve charge separation efficiency, and inhibit the recombination of photogenerated electrons and holes [19, 20].

Recently, g-C_3N_4, a polymeric metal-free semiconductor, has garnered significant research interest due to its excellent properties such as narrow bandgap (~2.7 eV), cost low, easy to prepare, non-toxic and suitable electronic band structure [21]. It can be synthesized through simple thermal polymerization from different N-rich precursors, namely melamine, dicyandiamide, urea, thiourea and cyanamide [22]. These properties of g-C_3N_4 help it gradually become an important photocatalyst in the field of environmental remediation [23]. Several studies have demonstrated enhanced photocatalytic dye degradation efficiency of composite materials like WO_3/g-C_3N_4 [24], Fe_2O_3/g-C_3N_4 [25], and CdS/g-C_3N_4 [26]. Recently, the synthesis of ZnO/g-C_3N_4 and TiO_2/g-C_3N_4 composite materials with photocatalytic activity under visible radiation has garnered significant research interest due to their effective separation of photogenerated electron-hole pairs and high charge transport capability [19, 20].

In this work, we focus on the synthesis and characterization of ZnO/g-C_3N_4 and TiO_2/g-C_3N_4 composite materials using a simple hydrolysis method at room temperature. Additionally, their photocatalytic activity was evaluated through the photodegradation capability of doxycycline (DC) in aqueous solution under visible light. Furthermore, the stability of the photocatalyst and the potential degradation mechanisms were also assessed.

2. Materials and Methods

2.1. Materials

The raw biomass of *P. australis* (cellulose 43.31%, hemicellulose 30.82%, and lignin 20.37%) was obtained as described in [27]. Several chemicals, including sodium hydroxide (NaOH, ≥ 99.0%), hydrochloric acid (HCl, 37%), potassium iodide (KI, ≥ 99.5%), potassium bromate ($KBrO_3$, 99.8%), urea ($CO(NH_2)_2$, > 99.0%), and sodium chloride (NaCl, ≥ 99.5%), were all sourced from Merck. Additional chemicals, such as zinc nitrate hexahydrate ($Zn(NO_3)_2{\cdot}6H_2O$, ≥ 99.0%), doxycycline hyclate ($C_{22}H_{24}N_2O_8{\cdot}HCl{\cdot}0.5H_2O{\cdot}0.5C_2H_6O$, 93.5%-HPLC), titanium(IV) oxysulfate ($TiOSO_4{\cdot}xH_2O$, ≥ 28% Ti), tert-Butanol ($(CH_3)_3COH$, t-BA, 99.5%), and L-ascorbic acid ($C_6H_8O_6$, AA, 99%) were sourced from Sigma-Aldrich. The chemicals were used directly upon receipt without any additional processing steps.

2.2. Methods

2.2.1. Synthesis of ZnO/ g-C_3N_4 and TiO_2/g-C_3N_4

First, a crucible containing 5.0 g of urea was placed in a tube furnace and subjected to pyrolysis at 520°C (heating rate: 3°C/min) for 2 h under a nitrogen atmosphere. The calcined product was then transferred entirely into a glass beaker containing 100 mL of distilled water and treated with ultrasound for 30 minutes. The solid was filtered and then dried at 105°C for 24 h, yielding pure g-C_3N_4 material (denoted as CN). Next, 7.437 g of $Zn(NO_3)_2{\cdot}6H_2O$ or 4.0 g of $TiOSO_4{\cdot}xH_2O$ was added to a 250 mL glass beaker containing 80 mL of distilled water, and the mixture was stirred with a magnetic stirrer until the salt completely dissolved. Then, 1.0 g of the previously prepared CN was added to each salt solution, and the mixture was

stirred continuously for 12 h on a magnetic stirrer at room temperature. Subsequently, 50 mL of 1.0 M NaOH solution was added dropwise to each beaker. The reaction mixture was allowed to hydrolyze for 4 h and then left to stand for 1 h. The precipitate was filtered and washed with distilled water, with the washing process repeated several times until the filtrate was nearly neutral. The obtained solid was dried at 105°C for 24 h, then finely ground and calcined in a tube furnace at 450°C (heating rate: 3°C/min) for 2 h under a nitrogen atmosphere, yielding the ZnO/CN and TiO_2/CN composite materials, designated as ZCN and TCN, respectively. For comparison, pure ZnO and TiO_2 samples were also synthesized under the same conditions in the absence of CN.

2.2.2. Characterization of materials

The structural properties of the material were analyzed by X-ray diffraction (XRD) using a Bruker D8 Advance X-ray diffractometer (Bruker, Germany) with CuK_α radiation (λ = 0.15401 nm) in the 2θ range from 10 to 80°. The morphology and particle size of the material were observed via scanning electron microscopy (SEM) using an FEI Nova NanoSEM 450 (USA) and transmission electron microscopy (TEM) with a JEOL JEM-1010 (USA). Elemental composition was determined by energy-dispersive X-ray spectroscopy (EDX) on a TEAM Apollo XL EDS (USA). Functional groups on the material surface were identified using Fourier-transform infrared spectroscopy (FTIR) on an IR Affinity-1S spectrometer (Shimadzu). The band gap values of the material were determined by UV-Vis diffuse reflectance spectroscopy (UV-Vis DRS) using a UV-2600 spectrophotometer (Shimadzu). Brunauer-Emmett-Teller (BET) surface area parameters were recorded using a TriStar 3000 V6.07A - Quantachrome device. Photoluminescence (PL) spectra of the samples were studied with a Horiba Fluorolog 3 FL3-22.

2.2.3. Photocatalytic Degradation of DC

In this experiment, 0.1 g of photocatalyst was added to a glass beaker containing 200 mL of a DC solution at a concentration of 10 $mg \cdot L^{-1}$. The photocatalytic system was equipped with a UV-cut filter (λ > 420 nm) and used a 50 W - 220 V Compact lamp (manufactured by Dien Quang, Vietnam) as the visible light source. The suspension mixture was stirred on a magnetic stirrer in the dark for 60 minutes to ensure that adsorption reached equilibrium. At specific time intervals, 5.0 mL of the reaction solution was withdrawn and centrifuged to determine the DC concentration. The DC concentrations before and after the reaction were measured by UV-Vis molecular absorption spectroscopy using a Spectro UV-2650 device (Labomed, USA) at λ_{max} = 346 nm [28]. The adsorption efficiency of DC (A%) was calculated according to the following expression:

$$A(\%) = \frac{(C_0 - C_{0e})}{C_0} \times 100 \quad (1)$$

in which C_0 ($mg.L^{-1}$) and C_{0e} ($mg.L^{-1}$) are the concentrations of the antibiotic at the initial time and at equilibrium, respectively.

The photodegradation efficiency of DC on the catalyst (D%) is calculated according to the equation below [29]:

$$D(\%) = \frac{(C_{0e} - C_t)}{C_{0e}} \times 100 \quad (2)$$

where C_t ($mg.L^{-1}$) represents the concentration of DC at the illumination time t (minutes). The photocatalytic degradation kinetics of DC on the catalyst can be described by the apparent first-order Langmuir–Hinshelwood kinetic equation as given below [29, 30]:

$$\ln \frac{C_t}{C_{0e}} = -kt \quad (3)$$

where k is the pseudo-first-order rate constant.

3. Results and Discussion

3.1. Characterization of samples

X-ray diffraction (XRD) was employed to analyze the crystal structure of ZnO, TiO_2, BC, ZCN, and TCN. As depicted in Fig. 1a, pure TiO_2 exhibited characteristic diffraction peaks at 25.2°, 37.7°, 48.1°, 53.8°, 54.8°, 62.6°, 68.7°, 70.4°, and 75.3° corresponding to the (101), (004), (200), (105), (211), (204), (116), (220), and (215) planes of the anatase phase of TiO_2 [31, 32]. The ZnO sample displays diffraction peaks at 2θ values of 31.9°, 34.7°, 36.5°, 47.5°, 56.8°, 62.7°, 66.6°, 67.9°, 69.1°, 72.9°, and 77.2°, corresponding to the (100), (002), (101), (102), (110), (103), (200), (112), (201), (004), and (202) planes of wurtzite ZnO (JCPDS No. 01-075-9743) [33, 34]. At 2θ values of 13.1° and 27.4°, corresponding to the (100) and (002) planes of g-C_3N_4, these peaks are also reported in previous studies [38-40]. Figure 1a further shows that both ZCN and TCN composites exhibit characteristic diffraction peaks similar to those of pure ZnO and TiO_2 materials. However, their diffraction intensities are lower, indicating the formation of the ZCN and TCN composites. The formation of these heterostructures likely inhibits the crystal growth of ZnO and TiO_2 within the ZCN and TCN composites. This is further supported by the calculated average crystallite size at (101): ZnO (37.0 nm), TiO_2 (13.8 nm), smaller for ZCN (27.6 nm), and TCN (6.9 nm) samples, respectively (Table 1).

Table 1: The parameters for crystal size (D), band gap (E_g), and BET surface area of the samples

Samples	ZnO	TiO_2	g-C_3N_4	ZCN	TCN
D (nm)	37.0	13.8	-	27.6	6.9
E_g (eV)	3.03	3.06	2.70	2.57	1.78
S_{BET} (m^2/g)	5.5	2.1	36.8	25.4	16.0
V_{pore} (cm^3/g)	0.021	0.009	0.166	0.151	0.127
D_{pore} (nm)	16.91	21.68	21.28	32.02	36.35

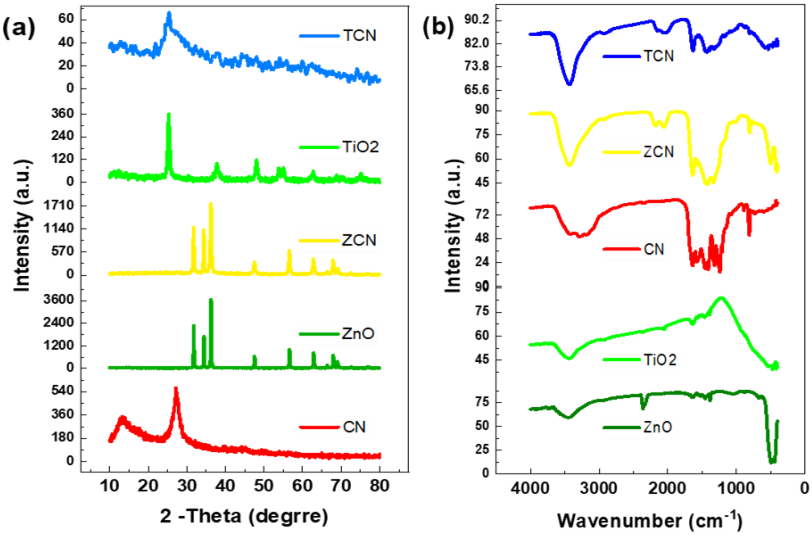

Figure 1: (a) The XRD patterns and (b) FTIR spectra of ZnO, TiO_2, CN, ZCN and TCN samples

The functional groups on the surface of the ZnO, TiO_2, CN, ZCN, and TCN materials were identified using FTIR spectroscopy, as shown in Figure 1b. The results indicated that all of the above samples exhibited absorption bands around 3400 cm^{-1} and 2350 cm^{-1}, which are attributed to the stretching vibrations of −OH in H_2O molecules and C−O in CO_2 molecules

adsorbed on the sample surface, respectively [35, 36]. For the ZnO and TiO_2 samples, absorption peaks at 498 cm^{-1} and 470 cm^{-1} were observed, corresponding to the stretching vibrations of the Zn−O and Ti−O bonds, respectively [37, 38]. For the CN sample, a broad absorption band between 3200 cm^{-1} – 3600 cm^{-1} was assigned to the stretching vibrations of N−H and O−H [36]. In addition, CN exhibited a series of characteristic stretching vibrations of the C−N ring (1636 cm^{-1}, 1459 cm^{-1}, and 1410 cm^{-1}) and bending vibrations of the tri-s-triazine unit (813 cm^{-1}) [36, 39]. The absorption peaks at 1317 cm^{-1} and 1240 cm^{-1} are C–N stretching vibrations associated with aromatic rings [39]. The ZCN and TCN composite samples also showed characteristic absorption peaks similar to those of the individual materials, but with lower absorption intensities. This further confirms the formation of heterostructures in the synthesized composites [40, 41].

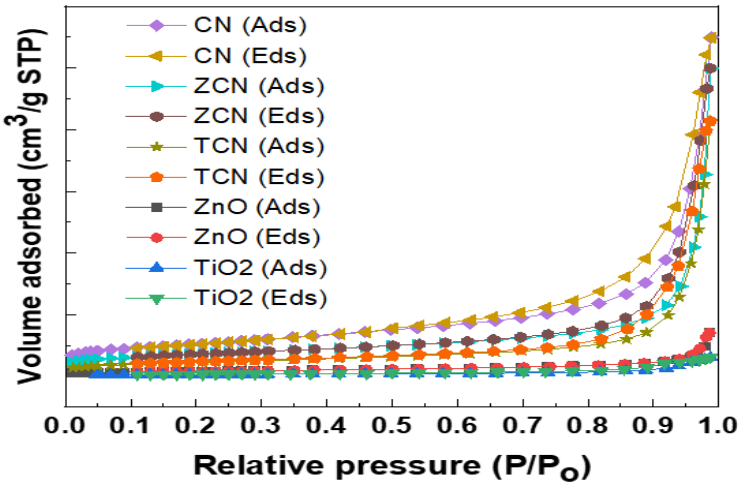

Figure 2: N_2 sorption/desorption isotherms of ZnO, TiO_2, CN, ZCN and TCN samples

The textural properties of ZnO, TiO_2, CN, ZCN, and TCN materials were examined by recording N_2 adsorption/desorption isotherms at 77 K (Fig. 2). As shown in Fig. 2, all the aforementioned samples exhibited type IV adsorption/desorption isotherms with an H3 hysteresis loop according to IUPAC classification, indicating that all these materials exist in a mesoporous structure [38, 42]. The specific surface area (S_{BET}) of pure ZnO, pure TiO_2 and pristine g-C_3N_4 were 5.5 m^2/g, 2.1 m^2/g and 36.8 m^2/g, respectively. When coupled with CN, the specific surface areas of ZCN and TCN composites were 25.4 m^2/g and 16.0 m^2/g, respectively (Table 1). This result shows that the loading of ZnO or TiO_2 nanoparticles on CN helped to improve the specific surface area for the obtained composites compared to the component materials. In general, the enhanced surface area could provide more potential active sites. The ZCN and TCN composite materials have higher specific surface areas compared to pure ZnO and TiO_2, respectively. This explains why these composites exhibit higher photodegradation efficiency of DC compared to pure ZnO and TiO_2. Furthermore, the incorporation of CN in the ZCN and TCN composites not only increases the specific surface area of the constituent materials but also forms heterostructures of ZnO/g-C_3N_4 or TiO_2/g-C_3N_4, which enhances the charge carrier transfer process in the composites, thereby improving their photocatalytic performance [43].

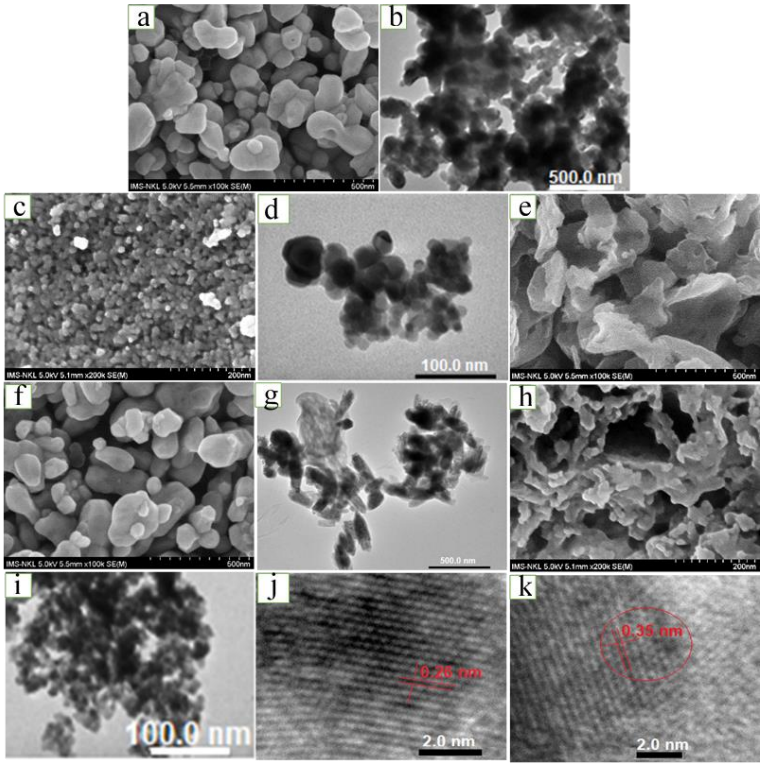

Figure 3: The SEM images of (a) ZnO, (c) TiO_2, (e) g-C_3N_4, (f) ZCN, and (h) TCN; the TEM images of (b) ZnO, (d) TiO_2, (g) ZCN, and (i) TCN; and the HRTEM images of (j) ZCN and (k) TCN

The morphology and microstructure of the ZnO, TiO_2, CN, ZCN, and TCN samples were thoroughly investigated using SEM and TEM techniques. SEM and TEM results reveal that both ZnO (SEM – Fig. 3a and TEM – Fig. 3b) and TiO_2 (SEM – Fig. 3c and TEM – Fig. 3d) exhibit spherical shapes, with aggregated particles having average diameters of approximately 35 nm and 15 nm, respectively. Figure 3e presents the SEM image of CN, showing a layered sheet structure that forms characteristic porous cavities. The composite samples ZCN (SEM – Fig. 3f and TEM – Fig. 3g) and TCN (SEM – Fig. 3h and TEM – Fig. 3i) contain spherical aggregates with sizes around 30 nm for ZCN and 10 nm for TCN, indicating the successful integration of these particles onto the surface of CN. High-resolution TEM (HRTEM) images of ZCN (Fig. 3j) and TCN (Fig. 3k) show lattice fringes with d-spacing values of 0.26 nm and 0.35 nm, corresponding to the (002) and (101) planes of ZnO wurtzite and TiO_2 anatase, respectively, as reported in previous studies [44, 45].

The elemental composition of the ZCN and TCN composite samples was analyzed using Energy Dispersive X-ray (EDX) spectroscopy, as shown in Figure 4. The analysis results revealed the presence of C, N, O, and Zn in the ZCN sample (Fig. 4a), and C, N, O, and Ti in the TCN sample (Fig. 4b). Additionally, elemental mapping analysis was performed to investigate the distribution of Zn, O, and Ti elements on the surface of the g-C_3N_4 nanosheets (Figure 4). In the selected scanning region where ZnO was present, Zn and O elements were detected (Fig. 4a), and in the area containing TiO_2, Ti and O elements were also found (Fig. 4b). Both the ZCN and TCN samples showed the presence of C and N elements. These results confirm that Zn, Ti, and O elements are uniformly distributed throughout the CN network, demonstrating the successful dispersion of ZnO and TiO_2 nanoparticles on CN.

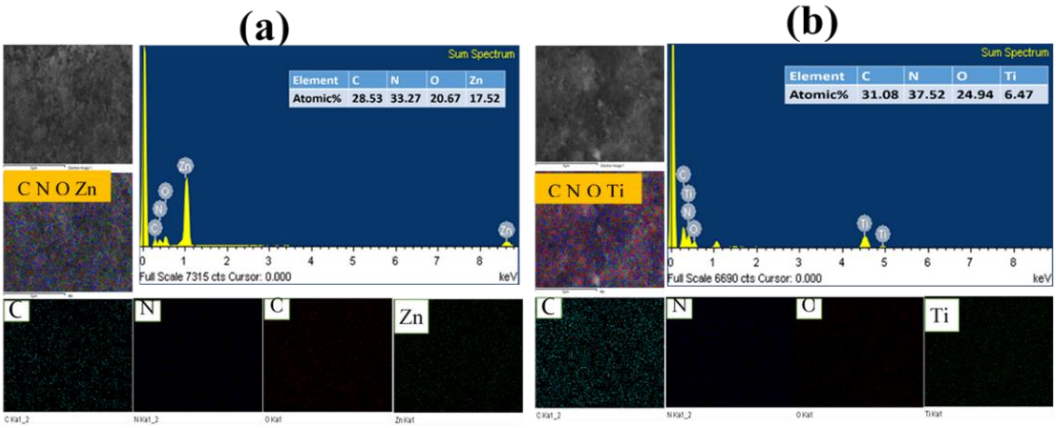

Figure 4: EDX elemental mapping of (a) ZCN, and (b) TCN

The optical properties of ZnO, TiO_2, CN, ZCN, and TCN samples were investigated using UV-Vis absorption spectroscopy in the wavelength range of 200 to 800 nm. As shown in Figure 5a, the pure ZnO, TiO_2, and CN samples exhibit absorption edges at wavelengths of 409 nm, 405 nm, and 459 nm, respectively. These results indicate that pure TiO_2 and ZnO strongly absorb UV radiation, while their absorption of visible light is weak [46, 47]. When ZnO or TiO_2 is dispersed on the surface of CN, the absorption edges of the ZCN and TCN composites shift red to wavelengths of approximately 482 nm and 696 nm, respectively. The bandgap energy of the samples can be calculated using the following equation [48]:

$$\lambda_g = \frac{1240}{E_g} \tag{4}$$

in this case, λ_g (nm) represents the absorption wavelength, and E_g (eV) is the band gap energy. The calculated values of E_g for the ZnO, TiO_2, CN, ZCN, and TCN samples are 3.03 eV, 3.06 eV, 2.70 eV, 2.57 eV, and 1.78 eV, respectively (see Table 1). The results show that the ZCN and TCN composites have significantly smaller band gaps compared to pure ZnO and TiO_2. This can be explained by the fact that g-C_3N_4 is a conductive polymer, and the incorporation of CN into the structure of ZnO or TiO_2 generates intermediate energy levels, thereby enhancing light absorption in both the UV and visible light regions. This implies that the recombination rate of photoinduced electron-hole pairs has been successfully reduced in the heterostructured ZnO/*g*-C_3N_4 and TiO_2/*g*-C_3N_4 composites [49].

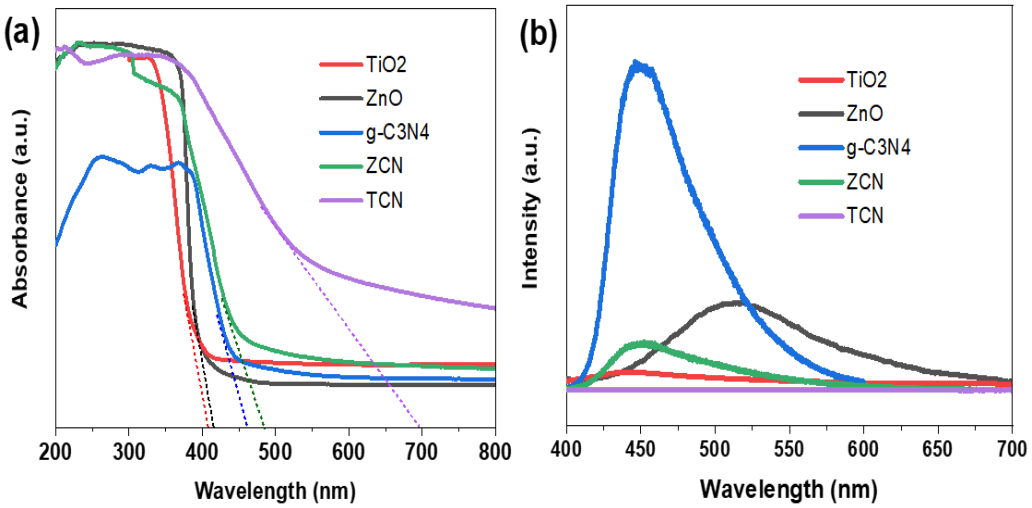

Figure 5: (a) UV–Vis DRS spectra, and (b) Photoluminescence spectra of ZnO, TiO_2, CN, ZCN and TCN samples

Photoluminescence (PL) spectroscopy has been employed to investigate the motion, transfer, and recombination processes of photogenerated electrons and holes in ZnO, TiO_2, CN, ZCN, and TCN samples. Figure 5b shows that the PL intensity of the composite samples ZCN and TCN is lower compared to ZnO and TiO_2, respectively. This result suggests that the coupling of g-C_3N_4 with ZnO or TiO_2 semiconductors may help prevent the recombination of photogenerated electrons and holes in the synthesized ZCN and TCN composite materials [40].

3.2. Photocatalytic degradation of samples

The photocatalytic degradation efficiency of DC on various materials, including ZnO, TiO_2, CN, ZCN, and TCN, under visible light irradiation is presented in Figure 6a. The results indicate that, in the absence of a photocatalyst, DC degradation did not occur within the 120-minute irradiation period, demonstrating the high stability of DC under the experimental conditions [30, 50].

For pure ZnO and TiO_2 samples, the photocatalytic degradation efficiency of DC was relatively low, reaching only 15.38% and 12.23%, respectively. In contrast, the CN material exhibited more promising photocatalytic activity in the visible light region, with a DC degradation efficiency of 60.58%. The high efficiency of g-C_3N_4 in the visible range has been confirmed in several previous studies [51, 52].

Among the materials tested, including ZnO, TiO_2, CN, ZCN, and TCN, TCN demonstrates a significant DC degradation efficiency of 89.75%, which is 7.34 times higher than that of pure TiO_2 and 1.48 times higher than pure CN. Notably, ZCN exhibits the highest efficiency, achieving a DC degradation rate of up to 97.02% after 120 minutes of illumination. Chemical oxygen demand (COD) evaluation for the initial DC solution (10 mg/L) was 8.0 mg/L, and after illumination on ZCN, the DC concentration was reduced to 0.31 mg/L. This result indicates that ZCN has the capability to fully mineralize DC (10 mg/L) in aqueous solution, highlighting its significant potential for environmental pollution treatment applications.

The photocatalytic degradation process of DC on ZnO, TiO_2, CN, ZCN, and TCN photocatalysts was evaluated using the apparent first-order kinetic equation (Eq. 3). As illustrated in the inset of Figure 5b, the photodegradation kinetics of DC for all examined samples followed a linear trend, indicating that the experimental data for DC degradation on these materials adhered to the apparent first-order kinetic model. Furthermore, it was observed that the apparent rate constants for the composite materials ZCN and TCN were significantly higher than those for the individual components ZnO, TiO_2, and CN (Fg. 6b). This result suggests that combining ZnO or TiO_2 with g-C_3N_4 can enhance the photocatalytic activity of the synthesized photocatalyst composites. Among the tested photocatalysts, the ZCN composite exhibited the highest apparent rate constant (Fig. 6b). The apparent rate constant values for ZnO, TiO_2, CN, ZCN, and TCN were 1.02×10^{-4} min^{-1}, 5.90×10^{-4} min^{-1}, 6.99×10^{-4} min^{-1}, 53.09×10^{-4} min^{-1}, and 35.15×10^{-4} min^{-1}, respectively. Comparison of the DC degradation rate constants for ZCN and TCN composites with previously reported experimental results suggests that the DC photodegradation rates for ZCN and TCN in this study are relatively high (Table 2).

Table 2: Apparent rate constant values for DC photodegradation on different catalysts

Catalyst	E_{bg} (eV)	Light source	C_0 (mg L^{-1}) /Vol. (mL) /$m_{catalyst}$ (mg)	k (min^{-1})	Refs.
ZnO/g-C_3N_4	2.57	50 W Compact lamp (λ > 420 nm)	10/200/100	0.05309	This study
TiO_2/g-C_3N_4	1.78	50 W Compact lamp (λ > 420 nm)	10/200/100	0.03515	This study
BiOCl/TiO_2	3.17	300 W Xenon lamp	20/100/50	0.0137	[53]
g-C_3N_4@CeO_2	2.75	150 W Xeon lamp (λ > 420 nm)	10/50/50	0.00381	[54]
TiO_2/Graphene/ZIF-8	-	LED lamp	450/100/9	0.007	[55]
$CoCr_2O_4$/α-Fe_2O_3/β-La_2S_3	2.50	1000 W Halogen lamp	10/20/50	0.0076	[56]
α-Bi_2O_3/g-C_3N_4/H_2O_2	-	150W Xenon lamp (λ > 420 nm)	10/50/25	0.014	[57]
g-C_3N_4/$Fe_2(MoO_4)_3$	-	350 W Xenon lamp	30/400/400	0.0207	[58]
g-C_3N_4/$Ni_{0.5}Zn_{0.5}Fe_2O_4$	2.35	Solar light	20/100/30	0.0415	[52]
Co/Mn-MOF-74@g-C_3N_4	1.73	300 W halogen lamp (λ > 420 nm)	40/40/50	0.00459	[59]

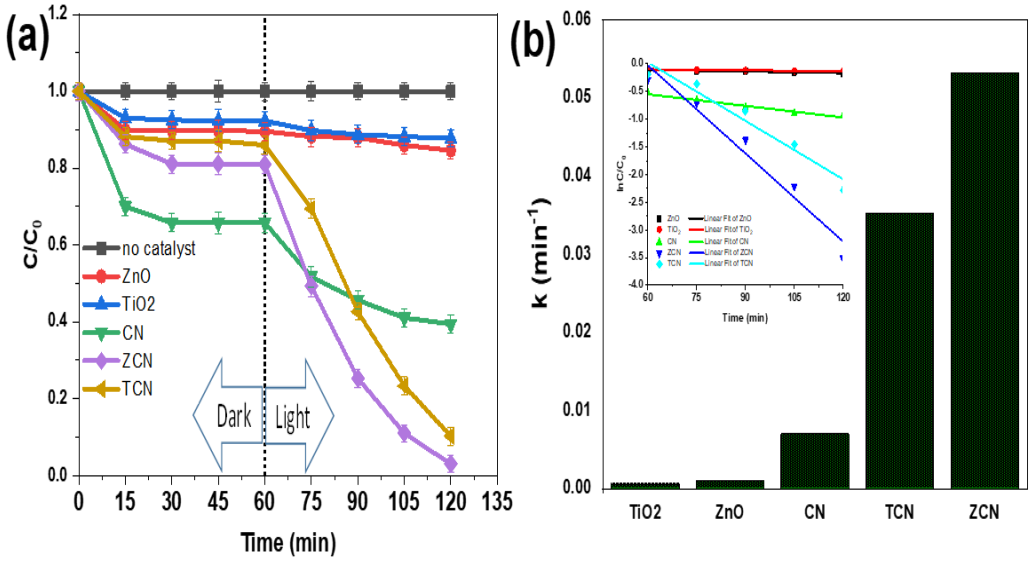

Figure 6: (a) DC photodegradation in the following cases: no catalyst, ZnO, TiO_2, CN, ZCN and TCN, and (b) Pseudo-first-order rate constant k (min^{-1}) of DC decomposition on ZnO, TiO_2, CN, ZCN and TCN samples

3.3. The influence of scavengers

Radicals such as h^+, e^-, $\bullet O_2^-$, and •OH are the primary reactive species in the photocatalytic degradation process of DC on ZCN and TCN composite materials. Radical scavenging experiments were conducted to investigate the role of these reactive species in the photocatalytic degradation of the antibiotic DC. In the experiments, solutions of potassium iodide (KI), potassium bromate ($KBrO_3$), tert-butanol (tBA), and ascorbic acid (AA) at a concentration of 10 mM were added to the DC solution to selectively scavenge h^+, e^-, •OH, and $\bullet O_2^-$ species, respectively [51, 60, 61]. The results indicate that the photocatalytic degradation efficiency of the ZCN sample decreased by 31.81%, 55.82%, 68.29%, and 79.81%, respectively, upon the addition of KI, $KBrO_3$, AA, and tBA (Fig. 7a). Similarly, the degradation efficiency of the TCN sample decreased by 11.61%, 43.51%, 74.18%, and 82.62% with the respective addition of radical scavengers (Fig. 7b).

First, the addition of tBA resulted in a significant decrease in DC degradation efficiency (79.81% for ZCN and 82.62% for TCN), suggesting that tBA plays a major role in inhibiting the formation of •OH radicals. Next, the addition of AA reduced the DC degradation

efficiency (68.29% for ZCN and 74.18% for TCN), indicating a considerable interference of AA in the formation of superoxide radicals $\bullet O_2^-$. Subsequently, $KBrO_3$, acting as an electron scavenger, decreased DC degradation efficiency by 55.82% for ZCN and 43.51% for TCN, implying a moderate inhibition of electrons. Finally, the photo-generated h^+ holes in both ZCN and TCN catalysts are secondary active species in the DC degradation process. Nevertheless, e^- and h^+ can also react with water and oxygen molecules adsorbed on the catalyst surface to generate •OH and $\bullet O_2^-$ radicals, which are introduced into the reaction system, contributing to the enhanced degradation efficiency of DC antibiotics in solution [40, 43].

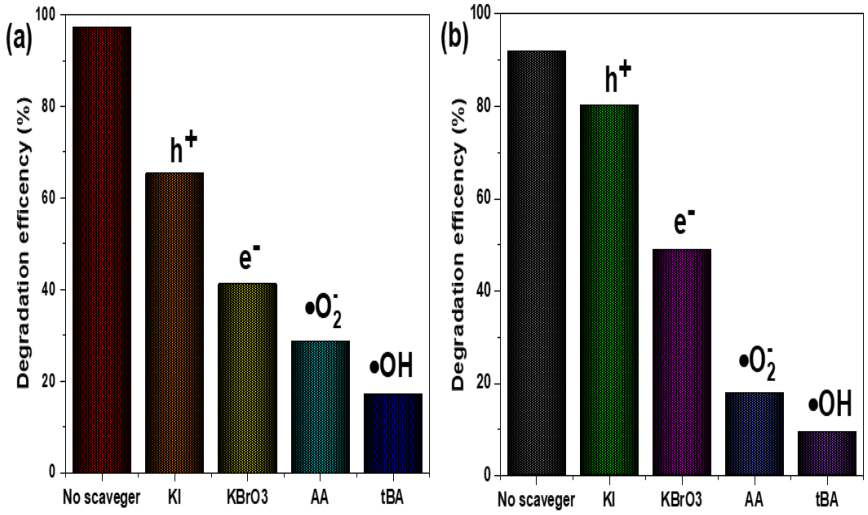

Figure 7: Effect of different scavengers on the photodegradation of DC over (a) ZCN and (b) TCN samples

The valence and conduction band-edge energies of photocatalytic semiconductors can be calculated by the equation below [62].

$$E_{VB} = \chi - E_e + 0.5E_g \quad (5)$$

$$E_{CB} = E_{VB} - E_g \quad (6)$$

wherre, χ represents the absolute electronegativity of the semiconductor. The χ values for the semiconductors g-C_3N_4, ZnO, and TiO_2 are 4.73 eV, 5.6 eV, and 5.81 eV, respectively [40, 62]. E_e denotes the energy of a free electron (4.5 eV relative to hydrogen), while E_g is the band gap energy of the semiconductor. The valence and conduction band edge energies of ZnO, TiO_2, and g-C_3N_4 are determined as (2.615 eV and -0.415 eV), (2.84 eV and -0.22 eV), and (1.58 eV and -1.12 eV), respectively. Thus, the differences in the valence band potential positions among ZnO, TiO_2, and g-C_3N_4 may lead to the formation of a type-II heterojunction effect [63].

Due to the wide band gap, the ZnO (3.03 eV) and TiO_2 (3.06 eV) catalysts are challenging to excite under visible light. Conversely, g-C_3N_4, with a narrower band gap (2.70 eV), can readily be excited by visible light, resulting in electron-hole pair generation (Eq. 7). These photogenerated electrons migrate to the catalyst surface and react with dissolved O_2 in solution, forming superoxide radicals $\bullet O_2^-$ (Eq. 8). The superoxide radicals further react with H_2O molecules and/or H^+ ions in solution to produce hydroperoxyl radicals •OH (Eqs. 9-12), which subsequently react with DC antibiotic molecules (Eq. 13) [40].

Because the conduction band potential of g-C_3N_4 (-1.12 eV) is more negative than that of ZnO (-0.415 eV) and TiO_2 (-0.22 eV), photogenerated electrons in the conduction band (CB) of g-C_3N_4 transfer to the CB of ZnO or TiO_2, subsequently migrating to the catalyst surface (Eq. 14) [64]. Furthermore, the valence band potentials of ZnO (2.615 eV) and TiO_2 (2.84

eV) are more positive than the potential of •OH/OH^- (1.99 eV) [65, 66], so the holes in the valence band of ZnO and TiO_2 cannot directly react with OH^- ions to form highly reactive hydroxyl radicals (•OH) [49, 67]. However, the VB potential of g-C_3N_4 (1.58 eV) is more negative than that of •OH/OH^- (1.99 eV) [65, 66], enabling the holes in the valence band of g-C_3N_4 to react with OH^- ions, generating active •OH radicals (Eq. 15). Due to their strong oxidative properties, these hydroxyl radicals interact with DC antibiotic molecules, resulting in decomposition products (Eq. 16) [40]. Furthermore, numerous studies demonstrate that h^+ vacancies in the valence band of g-C_3N_4 can directly oxidize DC antibiotic molecules (Eq. 16) [49, 67]. Based on the above interpretations and with reference to previously published studies [40, 64, 67, 68], a potential mechanism for the photocatalytic degradation of DC on heterogeneous catalysts such as ZCN or TCN under visible light irradiation can be proposed, as illustrated in Figure 8.

$$\text{ZCN or TCN} + h\nu \rightarrow \text{ZCN}\,(e^- + h^+) \text{ or TCN}\,(e^- + h^+) \quad (7)$$

$$g - C_3N_4(e^-) + \text{ZnO or } TiO_2 \rightarrow g - C_3N_4 + \text{ZnO}\,(e^-) \text{ or } TiO_2(e^-) \quad (8)$$

$$\text{ZCN}\,(e^-) \text{ or TCN}\,(e^-) + O_2 \rightarrow \text{ZCNB} + \bullet O_2^- \quad (9)$$

$$\bullet O_2^- + H^+ \rightarrow \bullet HO_2 + OH^- \quad (10)$$

$$\bullet O_2^- + H^+ \rightarrow \bullet HO_2 + OH^- \quad (11)$$

$$2\bullet HO_2 \rightarrow H_2O_2 + O_2 \quad (12)$$

$$H_2O_2 + e \rightarrow \bullet OH + OH^- \quad (13)$$

$$\text{ZnO}\,(h^+) \text{ or } TiO_2(h^+) + g - C_3N_4 \rightarrow \text{ZnO or } TiO_2 + g - C_3N_4(h^+) \quad (14)$$

$$g - C_3N_4\,(h^+) + OH^- \rightarrow g - C_3N_4 + \bullet OH \quad (15)$$

$$\bullet OH, h^+, \bullet O_2^- + \text{DC molecules} \rightarrow \text{DC decomposition products} \quad (16)$$

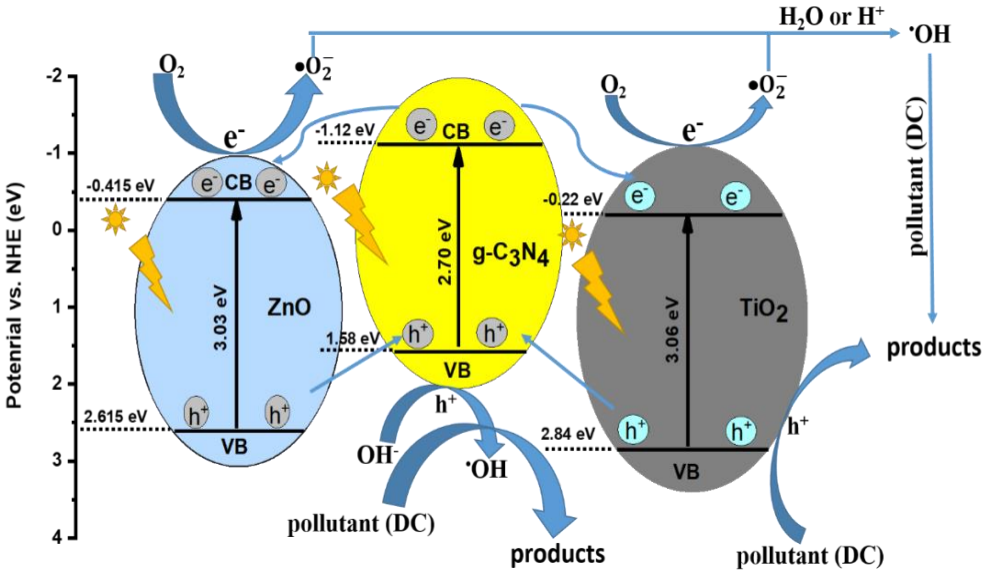

Figure 8: Schematic representation of the photocatalytic mechanism over ZCN and TCN

3.3. Recyclability and stability

To be effective in practical applications for treating polluted wastewater, photocatalysts must demonstrate long-term stability. Both the ZCN and TCN composite materials were tested for reusability over four cycles. After each test cycle, the photocatalysts were separated by centrifugation and desorbed multiple times using methanol to ensure near-complete removal of DC on the catalyst surfaces. Finally, the catalysts were dried at 105°C for 24 hours [69]. The photocatalytic degradation efficiency of DC on ZCN and TCN was observed to decrease from 97.02% to 89.14% and from 89.75% to 82.79%, respectively, after four cycles (Figures 9a and 9b). These results indicate that both photocatalysts exhibit relatively

high stability, though TCN appears slightly more stable than ZCN. The XRD patterns of ZCN and TCN samples before and after four reuse cycles show minimal changes, further demonstrating their structural stability (Figures 9c and 9d).

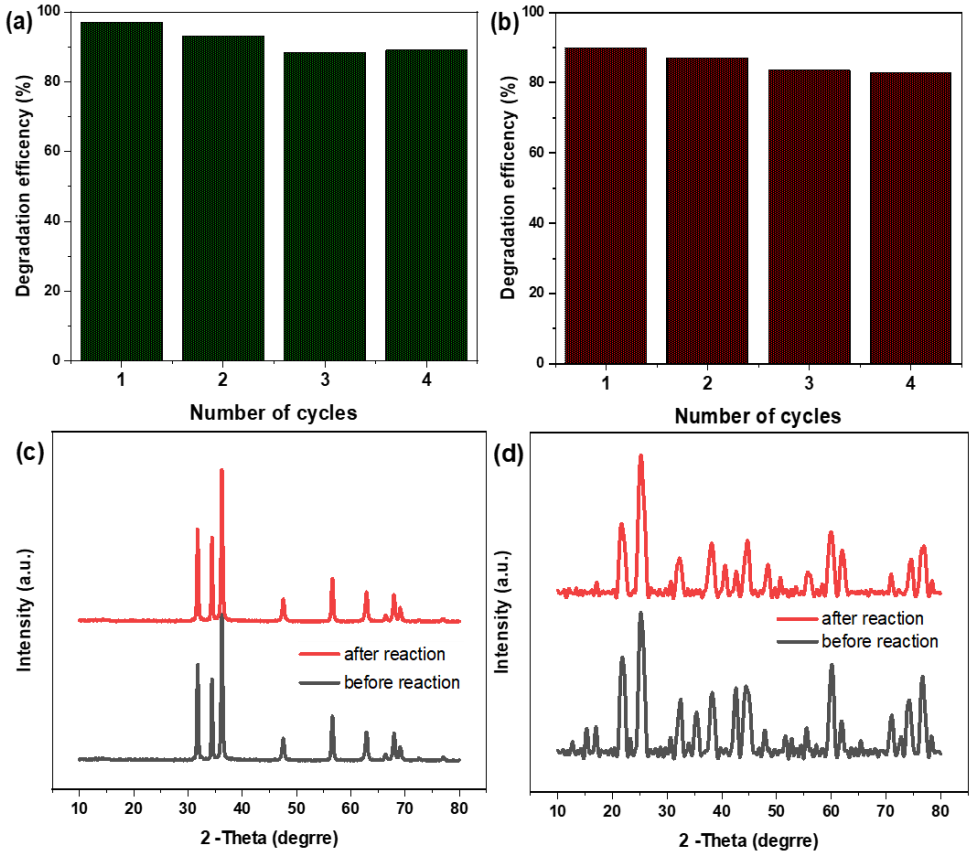

Figure 9: (a) and (b) the reusability of ZCN and TCN composites for four consecutive runs, respectively; and (c) and (d) XRD patterns for ZCN and TCN composites before and after reaction, respectively

Conclusion

In summary, the research team successfully synthesized second-generation composite materials, ZCN and TCN, as visible-light-responsive photocatalysts with significantly improved efficiency. The results demonstrated that ZnO nanoparticles (approximately 30–40 nm) and TiO_2 nanoparticles (around 10–15 nm) were uniformly dispersed across g-C_3N_4 nanosheets. The photocatalytic performance of the ZCN and TCN composites was markedly enhanced under visible light irradiation. Notably, the ZCN composite exhibited approximately 10% higher photocatalytic degradation capability compared to TCN and outperformed individual components such as ZnO, TiO_2, and g-C_3N_4. The enhanced photocatalytic efficiency of ZCN and TCN is attributed to the high photocatalytic activity of g-C_3N_4 and the effective separation of photogenerated electron-hole pairs within the heterostructured composite. The photocatalytic degradation of DC on both ZCN and TCN materials follows pseudo-first-order kinetics. The ZCN and TCN photocatalysts demonstrated stability during operation and show great potential for application in the photodegradation of various antibiotics in aqueous solutions.

Acknowledgments:

This research is supported by The Ministry of Education and Training under the project coded B2022.SPD.562.07.

Conflict of interest:

The authors declare no conflicts of interest.

References

[1] K. V. Karthik, A. V. Raghu, K. R. Reddy, R. Ravishankar, M. Sangeeta, N. P. Shetti, and C. V. Reddy, "Green synthesis of Cu-doped ZnO nanoparticles and its application for the photocatalytic degradation of hazardous organic pollutants," *Chemosphere,* vol. 287, no. Pt 2, p. 132081, 2022.

[2] G. Dong, B. Chen, B. Liu, L. J. Hounjet, Y. Cao, S. R. Stoyanov, M. Yang, and B. Zhang, "Advanced oxidation processes in microreactors for water and wastewater treatment: Development, challenges, and opportunities," *Water Research,* vol. 211, p. 118047, 2022.

[3] M. Pudukudy and Z. Yaakob, "Facile solid state synthesis of ZnO hexagonal nanogranules with excellent photocatalytic activity," *Applied Surface Science,* vol. 292, pp. 520-530, 2014.

[4] Z. Wang, Y. Wang, W. Zhang, Z. Wang, Y. Ma, and X. Zhou, "Fabrication of TiO_2(B)/Anatase Heterophase Junctions at High Temperature via Stabilizing the Surface of TiO_2(B) for Enhanced Photocatalytic Activity," *The Journal of Physical Chemistry C,* vol. 123, no. 3, pp. 1779-1789, 2019.

[5] R. Mohammed, M. E. M. Ali, E. Gomaa, and M. Mohsen, "Green ZnO nanorod material for dye degradation and detoxification of pharmaceutical wastes in water," *Journal of Environmental Chemical Engineering,* vol. 8, no. 5, p. 104295, 2020.

[6] V. Dutta, S. Sharma, P. Raizada, V. K. Thakur, A. A. P. Khan, V. Saini, A. M. Asiri, and P. Singh, "An overview on WO_3 based photocatalyst for environmental remediation," *Journal of Environmental Chemical Engineering,* vol. 9, no. 1, p. 105018, 2021.

[7] K. Yang, Z. Yang, C. Zhang, Y. Gu, J. Wei, Z. Li, C. Ma, X. Yang, K. Song, Y. Li, Q. Fang, and J. Zhou, "Recent advances in CdS-based photocatalysts for CO_2 photocatalytic conversion," *Chemical Engineering Journal,* vol. 418, p. 129344, 2021.

[8] A. K. Sibhatu, G. K. Weldegebrieal, S. Imteyaz, S. Sagadevan, N. N. Tran, and V. Hessel, "Synthesis and process parametric effects on the photocatalyst efficiency of CuO nanostructures for decontamination of toxic heavy metal ions," *Chemical Engineering and Processing - Process Intensification,* vol. 173, p. 108814, 2022.

[9] Z. Xu, C. Zhang, Y. Zhang, Y. Gu, and Y. An, "BiOCl-based photocatalysts: Synthesis methods, structure, property, application, and perspective," *Inorganic Chemistry Communications,* vol. 138, p. 109277, 2022.

[10] J. Wang, Z. Wang, B. Huang, Y. Ma, Y. Liu, X. Qin, X. Zhang, and Y. Dai, "Oxygen vacancy induced band-gap narrowing and enhanced visible light photocatalytic activity of ZnO," *ACS Appl Mater Interfaces,* vol. 4, no. 8, pp. 4024-4030, 2012.

[11] O. Carp, "Photoinduced reactivity of titanium dioxide," *Progress in Solid State Chemistry,* vol. 32, no. 1-2, pp. 33-177, 2004.

[12] M. Samadi, M. Zirak, A. Naseri, M. Kheirabadi, M. Ebrahimi, and A. Z. Moshfegh, "Design and tailoring of one-dimensional ZnO nanomaterials for photocatalytic degradation of organic dyes: a review," *Research on Chemical Intermediates,* vol. 45, no. 4, pp. 2197-2254, 2019.

[13] S.-C. Jung, K.-H. Chung, J. Choi, Y.-K. Park, S.-J. Kim, B.-J. Kim, and H. Lee, "Photocatalytic hydrogen production using liquid phase plasma from ammonia water over metal ion-doped TiO_2 photocatalysts," *Catalysis Today,* vol. 397-399, pp. 165-172, 2022.

[14] O. Dymshits, E. Gorokhova, I. Alekseeva, V. Golubkov, M. Shepilov, A. Khubetsov, M. Tsenter, D. Shemchuk, A. Bachina, A. Volokitina, L. Basyrova, M. Baranov, E. Oreschenko, X. Mateos, P. Loiko, and A. Zhilin, "Transparent materials based on semiconducting ZnO: glass-ceramics and optical ceramics doped with rare-earth and transition-metal ions," *Journal of Non-Crystalline Solids,* vol. 588, p. 121625, 2022.

[15] A. R. Agustin and K. Tamura, "Surface modification of TiO_2 nanoparticles with terephthalic acid in supercritical carbon dioxide," *The Journal of Supercritical Fluids,* vol. 174, p. 105245, 2021.

[16] Y. Y. Chan, Y. L. Pang, S. Lim, and W. C. Chong, "Facile green synthesis of ZnO nanoparticles using natural-based materials: Properties, mechanism, surface modification and application," *Journal of Environmental Chemical Engineering,* vol. 9, no. 4, p. 105417, 2021.

[17] J. Xia, H. Song, J. Yang, and X. Zhu, "Preparation of ellipsoid spheres interlaced flower-like g-C_3N_4/TiO_2 fluffy porous heterojunction and its visible-light photodegradation of organic pollutants," *Chemical Physics Letters,* vol. 824, p. 140524, 2023.

[18] P. Veisi, M. S. Seyed Dorraji, and M. H. Rasoulifard, "Effect of contact interface type in charge transfer mechanism and visible-light photocatalytic activity of ZnO-g-C_3N_4 heterostructures," *Materials Research Bulletin,* vol. 167, p. 112428, 2023.

[19] J. Wang, Z. Yang, X. Gao, W. Yao, W. Wei, X. Chen, R. Zong, and Y. Zhu, "Core-shell g-C_3N_4@ZnO composites as photoanodes with double synergistic effects for enhanced visible-light photoelectrocatalytic activities," *Applied Catalysis B: Environmental,* vol. 217, pp. 169-180, 2017.

[20] M. Vijayan, V. Manikandan, C. Rajkumar, A. A. Hatamleh, B. K. Alnafisi, G. Easwaran, X. Liu, K. Sivakumar, and H. Kim, "Constructing Z-scheme g-C_3N_4/TiO_2 heterostructure for promoting degradation of the hazardous dye pollutants," *Chemosphere,* vol. 311, p. 136928, 2023.

[21] G. Mamba and A. K. Mishra, "Graphitic carbon nitride (g-C_3N_4) nanocomposites: A new and exciting generation of visible light driven photocatalysts for environmental pollution remediation," *Applied Catalysis B: Environmental,* vol. 198, pp. 347-377, 2016.

[22] Y. Wang, S. Zhao, Y. Zhang, J. Fang, W. Chen, S. Yuan, and Y. Zhou, "Facile synthesis of self-Assembled g-C_3N_4 with abundant nitrogen defects for photocatalytic hydrogen evolution," *ACS Sustainable Chemistry & Engineering,* vol. 6, no. 8, pp. 10200-10210, 2018.

[23] K. Maeda, X. Wang, Y. Nishihara, D. Lu, M. Antonietti, and K. Domen, "Photocatalytic activities of graphitic carbon nitride powder for water reduction and oxidation under visible Light," *J. Phys. Chem. C,* vol. 113, pp. 4940–4947, 2009.

[24] L. Huang, H. Xu, Y. Li, H. Li, X. Cheng, J. Xia, Y. Xu, and G. Cai, "Visible-light-induced WO_3/g-C_3N_4 composites with enhanced photocatalytic activity," *Dalton Trans,* vol. 42, no. 24, pp. 8606-8616, 2013.

[25] Y. Xu, S. Huang, M. Xie, Y. Li, H. Xu, L. Huang, Q. Zhang, and H. Li, "Magnetically separable Fe_2O_3/g-C_3N_4 catalyst with enhanced photocatalytic activity," *RSC Advances,* vol. 5, no. 116, pp. 95727-95735, 2015.

[26] M. Lu, Z. Pei, S. Weng, W. Feng, Z. Fang, Z. Zheng, M. Huang, and P. Liu, "Constructing atomic layer g-C(3)N(4)-CdS nanoheterojunctions with efficiently enhanced visible light photocatalytic activity," *Phys Chem Chem Phys,* vol. 16, no. 39, pp. 21280-21288, 2014.

[27] B. T. M. Nguyet, N. H. Nghi, N. A. Tien, D. Q. Khieu, H. D. Duc, and N. V. Hung, "Enhanced adsorption of methylene blue by chemically modified materials derived from *Phragmites australis* stems," *Acta Chimica Slovenica* vol. 69, no. 4, pp. 811–825, 2022.

[28] W. Liu, J. Zhang, Q. Kang, H. Chen, and R. Feng, "Enhanced photocatalytic degradation performance of In_2O_3/g-C_3N_4 composites by coupling with H_2O_2," *Ecotoxicology and Environmental Safety,* vol. 252, p. 114611, 2023.

[29] P. Raizada, P. Singh, A. Kumar, G. Sharma, B. Pare, S. B. Jonnalagadda, and P. Thakur, "Solar photocatalytic activity of nano-ZnO supported on activated carbon or brick grain particles: Role of adsorption in dye degradation," *Applied Catalysis A: General,* vol. 486, pp. 159-169, 2014.

[30] J. Liu, S. Zhou, P. Gu, T. Zhang, D. Chen, N. Li, Q. Xu, and J. Lu, "Conjugate Polymer-clothed TiO_2@V_2O_5 nanobelts and their enhanced visible light photocatalytic performance in water remediation," *Journal of Colloid and Interface Science* vol. 578, pp. 402-411, 2020.

[31] D. Li, Y. Fang, J. Lu, J. Sun, X. Zhao, N. Hou, and J. Xing, "Enhanced biodegradation of PAHs by biochar and a TiO_2@biochar composite under light irradiation: Photocatalytic mechanism, toxicity evaluation and ecological response," *Chemical Engineering Journal,* vol. 458, p. 141495, 2023.

[32] R. Djellabi, B. Yang, Y. Wang, X. Cui, and X. Zhao, "Carbonaceous biomass-titania composites with Ti-O-C bonding bridge for efficient photocatalytic reduction of Cr(VI) under narrow visible light," *Chemical Engineering Journal,* vol. 366, pp. 172-180, 2019.

[33] M. Chen, C. Bao, D. Hu, X. Jin, and Q. Huang, "Facile and low-cost fabrication of ZnO/biochar nanocomposites from jute fibers for efficient and stable photodegradation of methylene blue dye," *Journal of Analytical and Applied Pyrolysis,* vol. 139, pp. 319-332, 2019.

[34] P. K. Bhargav, K. S. R. Murthy, J. K. Pandey, P. Mandal, M. S. Goyat, R. Bhatia, and A. Varanasi, "Tuning the structural, morphological, optical, wetting properties and anti-fungal

activity of ZnO nanoparticles by C doping," *Nano-Structures & Nano-Objects,* vol. 19, p. 100365, 2019.

[35] M. Samadi, H. A. Shivaee, M. Zanetti, A. Pourjavadi, and A. Moshfegh, "Visible light photocatalytic activity of novel MWCNT-doped ZnO electrospun nanofibers," *Journal of Molecular Catalysis A: Chemical,* vol. 359, pp. 42-48, 2012.

[36] L. Pi, R. Jiang, W. Zhou, H. Zhu, W. Xiao, D. Wang, and X. Mao, "g-C_3N_4 modified biochar as an adsorptive and photocatalytic material for decontamination of aqueous organic pollutants," *Applied Surface Science,* vol. 358, pp. 231-239, 2015.

[37] F. Guo, W. Shi, W. Guan, H. Huang, and Y. Liu, "Carbon dots/g-C_3N_4/ZnO nanocomposite as efficient visible-light driven photocatalyst for tetracycline total degradation," *Separation and Purification Technology,* vol. 173, pp. 295-303, 2017.

[38] M. S. Nasir, G. Yang, I. Ayub, S. Wang, and W. Yan, "Tin diselinide a stable co-catalyst coupled with branched TiO_2 fiber and g-C_3N_4 quantum dots for photocatalytic hydrogen evolution," *Applied Catalysis B: Environmental,* vol. 270, p. 118900, 2020.

[39] J. X. Sun, Y. P. Yuan, L. G. Qiu, X. Jiang, A. J. Xie, Y. H. Shen, and J. F. Zhu, "Fabrication of composite photocatalyst g-C_3N_4-ZnO and enhancement of photocatalytic activity under visible light," *Dalton Trans,* vol. 41, no. 22, pp. 6756-6763, 2012.

[40] S. Prabhu, M. Pudukudy, S. Harish, M. Navaneethan, S. Sohila, K. Murugesan, and R. Ramesh, "Facile construction of djembe-like ZnO and its composite with g-C_3N_4 as a visible-light-driven heterojunction photocatalyst for the degradation of organic dyes," *Materials Science in Semiconductor Processing,* vol. 106, p. 104754, 2020.

[41] P. Gholami, L. Dinpazhoh, A. Khataee, and Y. Orooji, "Sonocatalytic activity of biochar-supported ZnO nanorods in degradation of gemifloxacin: Synergy study, effect of parameters and phytotoxicity evaluation," *Ultrason Sonochem,* vol. 55, pp. 44-56, 2019.

[42] Z. Jiang, C. Zhu, W. Wan, K. Qian, and J. Xie, "Constructing graphite-like carbon nitride modified hierarchical yolk–shell TiO_2 spheres for water pollution treatment and hydrogen production," *Journal of Materials Chemistry A,* vol. 4, no. 5, pp. 1806-1818, 2016.

[43] X. Peng, M. Wang, H. Dai, F. Qiu, and F. Hu, "In situ growth of carbon nitride on titanium dioxide/hemp stem biochar toward 2D heterostructured photocatalysts for highly photocatalytic activity," *Environmental Science and Pollution Research,* vol. 27, no. 31, pp. 39198-39210, 2020.

[44] S. Cho, J.-W. Jang, J. S. Lee, and K.-H. Lee, "Carbon-doped ZnO nanostructures synthesized using vitamin C for visible light photocatalysis," *CrystEngComm,* vol. 12, no. 11, pp. 3929-3935 2010.

[45] S. Liang, M. An, S. Xia, B. Zhang, B. Xue, and G. Xu, "Enhanced photocatalytic degradation of methyl orange by TiO_2/biochar composites under simulated sunlight irradiation," *Optical Materials,* vol. 142, p. 114105, 2023.

[46] A. Kamal, M. H. Saleem, H. Alshaya, M. K. Okla, H. J. Chaudhary, and M. F. H. Munis, "Ball-milled synthesis of maize biochar-ZnO nanocomposite (MB-ZnO) and estimation of its photocatalytic ability against different organic and inorganic pollutants," *Journal of Saudi Chemical Society,* vol. 26, no. 3, p. 101445, 2022.

[47] H. Li, X. Meng, M. Zhen, and Z. Hu, "Rich oxygen vacancies-induced superior photocatalytic activities of TiO_2(B) ultrathin nanosheeets for the degradation of doxycycline hydrochloride under visible light," *Materials Letters,* vol. 330, p. 133363, 2023.

[48] D. Guo, D. Feng, Y. Zhang, Z. Zhang, J. Wu, Y. Zhao, and S. Sun, "Synergistic mechanism of biochar-nano TiO_2 adsorption-photocatalytic oxidation of toluene," *Fuel Processing Technology,* vol. 229, p. 107200, 2022.

[49] P.-Y. Kuang, Y.-Z. Su, G.-F. Chen, Z. Luo, S.-Y. Xing, N. Li, and Z.-Q. Liu, "g-C_3N_4 decorated ZnO nanorod arrays for enhanced photoelectrocatalytic performance," *Applied Surface Science,* vol. 358, pp. 296-303, 2015.

[50] F. Berdini, J. O. Otalvaro, M. Avena, and M. Brigante, "Photodegradation of doxycycline in water induced by TiO_2-MCM-41. Kinetics, TOC evolution and reusability," *Results in Engineering,* vol. 16, p. 100765, 2022.

[51] S. Swetha, M. A. Abdel-Maksoud, M. K. Okla, B. Janani, T. M. Dawoud, M. A. El-Tayeb, and S. Sudheer Khan, "Triple-mechanism driven Fe-doped n-n hetero-architecture of Pr_6O_{11}-MoO_3

decorated g-C_3N_4 for doxycycline degradation and bacterial photoinactivation," *Chemical Engineering Journal,* vol. 461, p. 141806, 2023.

[52] P. Dhiman, G. Rana, R. A. Alshgari, A. Kumar, G. Sharma, M. Naushad, and A. L. ZA, "Magnetic Ni-Zn ferrite anchored on g-C_3N_4 as nano-photocatalyst for efficient photo-degradation of doxycycline from water," *Environmental Research,* vol. 216, no. Pt 3, p. 114665, 2023.

[53] S. Bao, H. Liang, C. Li, and J. Bai, "A heterostructure BiOCl nanosheets/TiO_2 hollow-tubes composite for visible light-driven efficient photodegradation antibiotic," *Journal of Photochemistry and Photobiology A: Chemistry,* vol. 397, p. 112590, 2020.

[54] W. Liu, J. Zhou, and Z. Hu, "Nano-sized g-C_3N_4 thin layer @ CeO_2 sphere core-shell photocatalyst combined with H_2O_2 to degrade doxycycline in water under visible light irradiation," *Separation and Purification Technology,* vol. 227, p. 115665, 2019.

[55] B. Rabeie and N. M. Mahmoodi, "Hierarchical ternary titanium dioxide decorated with graphene quantum dot/ZIF-8 nanocomposite for the photocatalytic degradation of doxycycline and dye using visible light," *Journal of Water Process Engineering,* vol. 54, p. 103976, 2023.

[56] P. R. Sivaranjani, A. Syed, A. M. Elgorban, A. H. Bahkali, R. Balakrishnaraja, R. S. Varma, and S. Sudheer Khan, "Fabrication of ternary nano-heterojunction via hierarchical deposition of α-Fe_2O_3 and β-La_2S_3 on cubic $CoCr_2O_4$ for enhanced photodegradation of doxycycline," *Journal of Industrial and Engineering Chemistry,* vol. 118, pp. 407-417, 2023.

[57] W. Liu, Z. Li, Q. Kang, and L. Wen, "Efficient photocatalytic degradation of doxycycline by coupling alpha-Bi_2O_3/g-C_3N_4 composite and H_2O_2 under visible light," *Environ Res,* vol. 197, p. 110925, 2021.

[58] V. Vasanthakumar, M. Alsawalha, K. Jothimani, M. L. Fu, and B. Yuan, "Z-scheme direct dual semiconductor photocatalytic system with porous g-C_3N_4/$Fe_2(MoO_4)_3$ composite: A promising approach for enhanced photocatalytic degradation of doxycycline," *Journal of Environmental Chemical Engineering,* vol. 12, no. 1, p. 111710, 2024.

[59] Q. Wen, D. Li, H. Li, M. Long, C. Gao, L. Wu, F. Song, and J. Zhou, "Synergetic effect of photocatalysis and peroxymonosulfate activated by Co/Mn-MOF-74@g-C_3N_4 Z-scheme photocatalyst for removal of tetracycline hydrochloride," *Separation and Purification Technology,* vol. 313, p. 123518, 2023.

[60] S. Preetha, S. Ramamoorthy, R. Pillai, B. Narasimhamurthy, and I. C. Lekshmi, "Influence of Lanthanum-doping on photocatalytic activity of magnetic $BiFeO_3$ nanocrystals for sunlight driven degradation of metachrome yellow," *Materials Today: Proceedings,* vol. 62, pp. 5396-5401, 2022.

[61] A. Iqbal, U. Saidu, S. Sreekantan, M. N. Ahmad, M. Rashid, N. M. Ahmed, W. H. Danial, and L. D. Wilson, "Mesoporous TiO_2 Implanted ZnO QDs for the photodegradation of tetracycline: Material design, structural characterization and photodegradation mechanism," *Catalysts,* vol. 11, no. 10, p. 1205, 2021.

[62] L. Ma, G. Wang, C. Jiang, H. Bao, and Q. Xu, "Synthesis of core-shell TiO_2@g-C_3N_4 hollow microspheres for efficient photocatalytic degradation of rhodamine B under visible light," *Applied Surface Science,* vol. 430, pp. 263-272, 2018.

[63] Y.-C. Shi, S.-S. Chen, J.-J. Feng, X.-X. Lin, W. Wang, and A.-J. Wang, "Dicationic ionic liquid mediated fabrication of Au@Pt nanoparticles supported on reduced graphene oxide with highly catalytic activity for oxygen reduction and hydrogen evolution," *Applied Surface Science,* vol. 441, pp. 438-447, 2018.

[64] W. Liu, M. Wang, C. Xu, and S. Chen, "Facile synthesis of g-C_3N_4/ZnO composite with enhanced visible light photooxidation and photoreduction properties," *Chemical Engineering Journal,* vol. 209, pp. 386-393, 2012.

[65] B. Lin, C. Xue, X. Yan, G. Yang, G. Yang, and B. Yang, "Facile fabrication of novel SiO_2/g-C_3N_4 core–shell nanosphere photocatalysts with enhanced visible light activity," *Applied Surface Science,* vol. 357, pp. 346-355, 2015.

[66] W. Wang, J. C. Yu, D. Xia, P. K. Wong, and Y. Li, "Graphene and g-C_3N_4 nanosheets cowrapped elemental alpha-sulfur as a novel metal-free heterojunction photocatalyst for bacterial inactivation under visible-light," *Environ Sci Technol,* vol. 47, no. 15, pp. 8724-8732, 2013.

[67] H. Lv, G. Ji, Z. Yang, Y. Liu, X. Zhang, W. Liu, and H. Zhang, "Enhancement photocatalytic activity of the graphite-like C_3N_4 coated hollow pencil-like ZnO," *Journal of Colloid and Interface Science,* vol. 450, pp. 381-387, 2015.

[68] M. Mousavi and A. Habibi-Yangjeh, "Magnetically separable ternary g-C_3N_4/Fe_3O_4/BiOI nanocomposites: novel visible-light-driven photocatalysts based on graphitic carbon nitride," *Journal of Colloid and Interface Science,* vol. 465, pp. 83-92, 2016.

[69] C. He, J. Ma, H. Xu, C. Ge, and Z. Lian, "Selective capture and determination of doxycycline in marine sediments by using magnetic imprinting dispersive solid-phase extraction coupled with high performance liquid chromatography," *Marine Pollution Bulletin* vol. 184, p. 114215, 2022.